Liquid Crystals
Publication details, including instructions for authors and subscription information:
http://www.informaworld.com/smpp/title~content=t713926090

Twist-grain-boundary phase diagrams in chiral liquid crystals

C. W. Garland

Online publication date: 06 August 2010

To cite this Article Garland, C. W.(1999) 'Twist-grain-boundary phase diagrams in chiral liquid crystals', Liquid Crystals, 26: 5, 669 — 677
To link to this Article: DOI: 10.1080/026782999204723
URL: http://dx.doi.org/10.1080/026782999204723

LIQUID CRYSTALS, 1999, VOL. 26, NO. 5, 669–677

Twist-grain-boundary phase diagrams in chiral liquid crystals

C. W. GARLAND

Department of Chemistry and Center for Material Science and Engineering,
Massachusetts Institute of Technology, Cambridge, Massachusetts 02139, USA

(*Received 17 September 1998; accepted 11 November 1998*)

The experimental phase diagrams of several chiral systems are compared with a theoretical diagram based on the chiral Chen–Lubensky model, which predicts at least two kinds of twist-grain-boundary phase, TGB_A and TGB_C. Also shown for comparison are typical nonchiral phase diagrams that exhibit a nematic–smectic A–smectic C multicritical point. Several aspects of experiment and theory agree, but there appear to be common experimental features that differ from those predicted by current theory.

1. Introduction

A twist-grain-boundary (TGB) phase of a chiral liquid crystal exhibits simultaneously a helical twist and blocks of smectic layering. Depending on the character of these smectic blocks (SmA = smectic A, SmC = smectic C, SmC* = smectic C*), TGB_A, TGB_C, and TGB_{C^*} phases are predicted. TGB_A phases were predicted theoretically by Renn and Lubensky [1, 2] and first observed experimentally by Goodby and coworkers [3–7]. Subsequently, other TGB_A systems were reported and studied in some detail [8–10]. TGB_C phases were then predicted [11, 12], and first observed experimentally by Nguyen and coworkers [9, 13, 14]. Further experimental information on both TGB_A and TGB_C systems is given in [15, 16].

The early work on TGB_A phases was carried out on the compounds nP1M7 (methylheptyl-alkoxyphenyl-propioloyloxybiphenyl carboxylate) [3–7], which exhibit the phase sequence SmC*–TGB_A–I, (I = isotropic) whereas later work on the series nFBTFO$_1$M$_7$ and nF$_2$BTFO$_1$M$_7$ [8–10, 13–16] revealed the sequences SmC*–SmA–TGB_A–N*–I or SmC*–TGB_A–N*–I, (N* is the cholesteric or twisted nematic phase). [Note that the presence of various blue phases (BP) are largely neglected in this presentation.] The latter sequences correspond to those predicted [2] for systems with TGB_A phases. Also work on nF$_2$BTFO$_1$M$_7$ for larger n values revealed the sequence SmC*–TGB_C^{α}–TGB_C^{β}–N*–I [14]. The structural formula for these two chiral tolan derivatives is

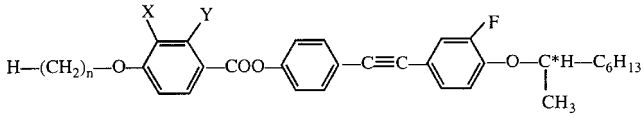

where X = F and Y = H for nFBTFO$_1$M$_7$ and X, Y = F for nF$_2$BTFO$_1$M$_7$. The chemical name of nFBTFO$_1$M$_7$ is 3-fluoro-4[(*R*) or (*S*)-1-methylheptyloxyl]4′-(4-alkoxy-3-fluorobenzoyloxy)tolan, and nF$_2$BTFO$_1$M$_7$ is the 2,3-difluorobenzoyloxy analogue.

The goal of the present work is to show the evolution from the N–SmA–SmC phase diagram of non-chiral compounds to phase diagrams involving TGB_A and TGB_C phases as chirality is introduced. Enough published high-resolution work is now available to show several general experimental trends and to allow a comparison with Renn–Lubensky predictions [1, 2, 11, 12] based on a chiral Chen–Lubensky model and augmented by the twisted chiral nematic line liquid (denoted here as N_L^*) behaviour introduced by Kamien and Lubensky [17].

The analogy between chiral liquid crystals and high T_c type-II superconductors in a field is very close: Meissner phase↔SmA, Abrikosov vortex flux lattice↔TGB_A, Abrikosov vortex liquid↔N_L^*, normal metal↔N*. The additional liquid crystal phases SmC* and TGB_C arise when the coefficient $c_\perp$ of the order parameter gradient-squared free energy term becomes negative. For a non-chiral system, $c_\perp > 0$ corresponds to SmA, $c_\perp < 0$ corresponds to SmC, and the locus $c_\perp = 0$ is the SmA–SmC transition line. There is no superconductor analogue for the distinction between SmA and SmC* or between TGB_A and TGB_C.

Section 2 is a brief review of nonchiral N–SmA–SmC phase diagrams; §3 summarizes the Renn–Lubensky theoretical results for the topology of TGB phase diagrams in chiral systems. Section 4 presents a series of experimental phase diagrams and compares these with the behaviour predicted by current theory. Finally, §5 stresses the apparently universal aspects of the present experiments and lists the unresolved problems which remain as a challenge to both theory and experiment.

2. Nonchiral N–SmA–SmC diagrams

Two typical nonchiral systems that exhibit a N–SmA–SmC multicritical point are shown in figures 1 and 2.

Journal of Liquid Crystals ISSN 0267-8292 print/ISSN 1366-5855 online
http://www.tandf.co.uk/JNLS/lct.htm
http://www.taylorandfrancis.com/JNLS/lct.htm

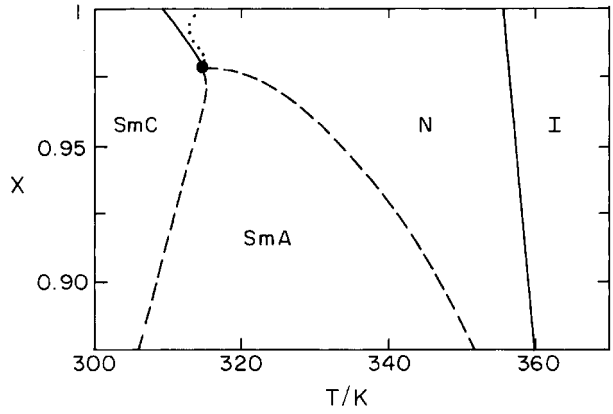

Figure 1. Partial phase diagram in the N–SmA–SmC region for mixtures of 7S5 and 8OCB [18, 19]. X is the mole fraction of 7S5. The dashed lines represent second order transitions, and solid lines are first order transitions. The locus of $c_\perp = 0$ is shown by a dotted line in the immediate vicinity of the N–SmA–SmC point [18].

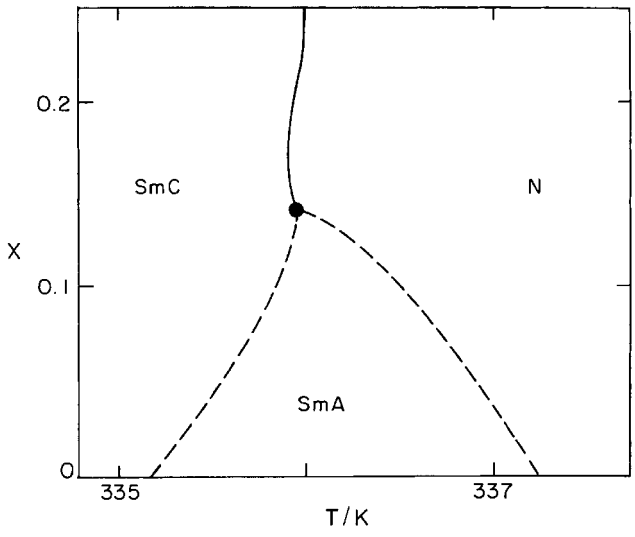

Figure 2. Partial phase diagram in the N–SmA–SmC region for 5O8 + 6O8 mixtures [21]. X is the weight fraction of 6O8. Dashed lines are second order transitions, and the solid N–SmC line is first order.

Both high-resolution X-ray [18] and heat capacity [19] studies are available for 7S5 + 8OCB (heptyloxypentylphenyl thiolbenzoate + octyloxycyanobiphenyl) mixtures, as is also true for 7S5 + 8S5 mixtures [20] (not shown). For the 5O8 + 6O8 (alkyloxyphenyl octyloxybenzoates) mixtures, there are unusually complete calorimetric results including first order latent heats as well as $C_p(T)$ data [21].

The positions of the phase boundaries near the N–SmA–SmC point in these two mixtures conform well with the universal nonchiral N–SmA–SmC phase topology established empirically in mixtures by Brisbin *et al.* [22] and confirmed by Shashidhar *et al.* [23] in pressure studies of pure compounds. (See [18] for such an analysis of the 7S5 + 8OCB system.) The nature of the N–SmA–SmC multicritical point is not fully understood since it has both a Lifshitz-point character [18], as expected from the Chen–Lubensky model [24], and also a Landau mean-field tricritical character, as shown by calorimetric data [19 *a*, 21, 25]. It is surprising that the free energy coefficients C of the ψ^4 term and $c_\perp$ of the gradient-squared $(\nabla\psi)^2$ term both vanish at the same point, but this is shown by high-resolution experiments to be true within quite narrow resolution limits. To summarize the nature of the three phase transitions: (a) the N–SmC transition is first order, as expected from general theoretical arguments [26], with the latent heat becoming zero at or very near the N–SmA–SmC point [21] and a Landau mean-field excess heat capacity in the SmC phase that grows on approach to the N–SmA–SmC point [19 *a*, 20 *a*, 21]; (b) the SmA–SmC transition is second order of the Landau mean-field type with the magnitude of the excess heat capacity ΔC_p at the transition diverging as the N–SmA–SmC point is approached [20 *a*, 21]; (c) the N–SmA transition is second order but fluctuation-dominated with an effective critical exponent α that varies with composition for two reasons—(1) crossover between 3D–XY and Gaussian-tricritical limits and (2) Fisher renormalization due to the large values of $(\mathrm{d}T_{\mathrm{NA}}/\mathrm{d}X)^2$, where X is the mole fraction in binary mixtures [19 *b*, 27].

Although there are many attractive and successful aspects of the Chen–Lubensky (CL) model of nonchiral N–SmA–SmC systems [24], there are several remaining theoretical difficulties. As mentioned above, the multicritical point has Landau tricritical character as well as Lifshitz character. The mean-field CL model predicts that all three transitions are second order, whereas the N–SmC transition is always first order as discussed above. The univeral phase topology has been modelled empirically but not derived from any theoretical model. Finally, the experimental locus of $c_\perp = 0$ in the N phase near the N–SmA–SmC point lies very close to the N–SmC transition line, as shown in figure 1, whereas the CL diagram shows the N–SmC line extending to large negative $c_\perp$ values.

3. Theoretical TGB phase diagrams

The initial conception of TGB phases [1] flowed from the early de Gennes analogy between the smectic liquid crystal free energy functional and the Landau–Ginzburg free energy for superconductors, augmented by an analysis similar to that used for Abrikosov flux lattices. The earliest detailed chiral CL theory of the phase diagram was a mean-field treatment for the case $c_\perp > 0$ [2], and it was shown that a $\mathrm{TGB_A}$ phase was stable

between the N* and SmA phases if the quantity $\lambda/\xi > 1/\sqrt{2}$, where λ is the twist penetration depth and ξ is the smectic coherence length. Thus a TGB_A phase would be expected near a N*–SmA–SmC* point since $\lambda \to \infty$ along the SmA–SmC* boundary and along the $c_\perp = 0$ locus in the N* phase.

The next theoretical step involved a mean-field treatment of the chiral CL model for $c_\perp < 0$ as well as $c_\perp > 0$ [11, 12]. One result of this model was the phase diagram shown in figure 3, which shows stable TGB_A and TGB_C phases. The TGB_C phase occurs for negative $c_\perp$: the point L in figure 3 is at $c_\perp = 0$ and the point B_3 is at a small negative $c_\perp$ value. The smooth matching of the N_L^*–TGB_A and N_L^*–TGB_C boundaries at L is a rigorous result for the linearized Chen–Lubensky equations. In [12] it is also shown that there can be a second tilted TGB phase—TGB_{C^*}—if *both* the splay and twist Frank elastic constants K_1 and K_2 are larger than the bend constant K_3. In this case (see figures 12 and 13 of [12]), the TGB_{C^*} phase is smaller in extent and lies at lower temperatures than TGB_C, i.e. lies just above the SmC* phase.

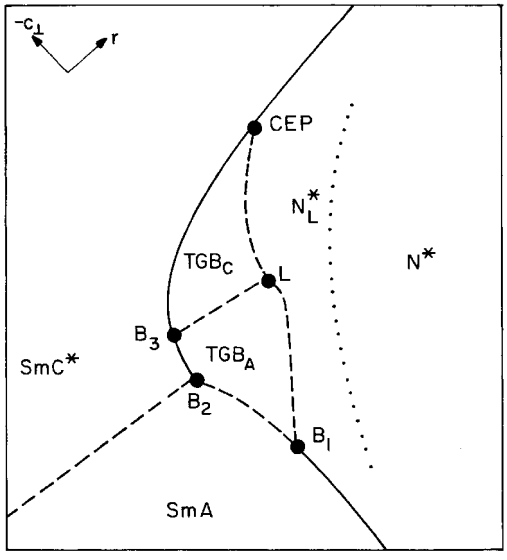

Figure 3. Theoretical TGB phase diagram given in [12] for chiral systems with an underlying N*–SmA–SmC* topology, showing the location of stable TGB_A and TGB_C phases. The theoretical axes $r \sim (T - T_{NAC})$ and $c_\perp$ have been rotated to display this theoretical topology in a way that best matches experimental plots of temperature (horizontal axis) versus composition (vertical axis). The dashed lines represent transitions predicted in the mean-field approximation to be second order, and the solid lines are predicted to be first order [12]. The dotted line is not a thermodynamic transition but represents the estimated location of the locus of maxima in the response functions for the N*–N_L^* change in short range order [17]. The multicritical point labels B_1–B_3, L, and CEP are taken from [12].

The dotted line in figure 3 has been added to the diagram obtained from [12] on the basis of a later theoretical development by Kamien and Lubensky [17]. The latter predicted a twisted chiral nematic line liquid N_L^* with *short range* TGB order. This is exactly analogous to the Abrikosov vortex *liquid* in superconductors. It must be stressed that the N*–N_L^* dotted line is not a thermodynamic transition line but represents the locus of finite maxima in the thermodynamic response functions. Such a locus has been established experimentally from detailed calorimetric studies that yield a broad C_p peak at temperatures above those where TGB phases occur [10, 14]; see also recent X-ray data [28] concerning the N_L^* region. Since the theory in [17] does not predict the location of this locus, it has been assumed to lie in the N* region roughly parallel to the TGB phase boundaries but extending beyond points B_1 and CEP in figure 3.

More recently, extensions have been made of the Renn–Lubensky theoretical model by Dozov [29] and Luk'yanchuk [30]. The work of Luk'yanchuk considers four TGB_C phases—TGB_{Cp}, TGB_{Ct}, TGB_{2q}, and TGB_{C^*}. The original TGB_C phase proposed in [11, 12] was TGB_{Cp}, where the smectic layers are parallel to the pitch axis. However, X-ray experiments [13] and recent theory [29, 30] show that TGB_{Ct}, with smectic layers tilted with respect to the pitch axis, is more stable than TGB_{Cp} [31]. If the novel TGB_{2q} phase exists, it is predicted to lie at higher temperatures than the TGB_{Ct} phase. Since neither the TGB_{C^*} nor TGB_{2q} phases are yet confirmed experimentally, they are not shown in figure 3 where the field labelled TGB_C should be understood to be a TGB_{Ct} phase.

The predicted order of the various phase transitions is shown in figure 3 by dashed lines for second order and solid lines for first order. Thus the theoretical multicritical points are bicritical points (B_1 and B_2), unknown type (L), and critical end points (B_3 and CEP). As shown in §4, experiments do not agree with these predictions. Thus either fluctuation effects are important or there are underlying problems with the basic Chen–Lubensky N–SmA–SmC model.

Theoretically there should always be a TGB phase in chiral N*–SmA–SmC* systems since λ/ξ diverges at the N*–SmA–SmC* point and thus $\lambda/\xi > 1/\sqrt{2}$. However, if the chiral field h is small, where $h \equiv k_0 K_2 = (2\pi/P)K_2$ (k_0 is the twist wave vector, and P is the pitch in the N* phase), then the maximum extent of the TGB_A phase will also be small [2, 12] and one might not resolve experimentally the presence of a TGB phase. Thus in practice the prospect of observing TGB phases experimentally will be best when the chirality (density conjugate to h) is largest. As a measure of the chirality, it seems reasonable to take the value of $k_0 = 2\pi/P$ (which

is analogous to the magnetic flux density) in the N* phase far from any TGB phase. This k_0 value has been determined near the N*–I transition (actually N*–BP_I in many cases). Also of value is the quantity $(k_0/q_0)^{2/3}$, where q_0 is smectic wave vector $2\pi/d$ and d is the smectic layer thickness [2, 12]. The latter ratio determines the theoretically estimated *maximum* width $\Delta T(\max)$ of the TGB_A phase:

$$\Delta T(\max) \simeq (T_{NA}-T_{B_2}) \simeq T_{NA} B (k_0/q_0)^{2/3} \qquad (1)$$

where T_{NA} is the N–SmA transition temperature at the fictive N*–SmA–SmC* point that would occur if no TGB_A phase appeared, and B is a constant of order unity [2, 12]. With typical experimental values of $0.01 < k_0/q_0 < 0.02$, $T_{NA} \simeq 370$ K and the assumed value $B = 1$, equation (1) yields $\Delta T(\max) \simeq 17$–27 K, which is too large to agree with experimental values. B values of ~ 0.2 would yield better agreement, as shown by $\Delta T(\max)$ values given in the next section.

Finally, it should be noted that there is no role for the isotropic phase in the theoretical models discussed above. However, high temperature truncation by I can occur, yielding SmA–I or SmC*–I transitions where the N* and TGB phases disappear. Experimental examples of such behaviour are mentioned in §4.

4. Chiral N*–SmA–SmC* diagrams

Three experimental phase diagrams are presented and discussed in this section. The first system, shown in figure 4, involves a binary mixure of two chiral compounds MDW74 + W82; MDW74 is 4-[(2*R*, 3*R*)-epoxyhexyloxy]phenyl 4-[(3*S*, 7)-dimethyloctyloxy]benzoate and W82 is 4[(*S*)-(4-methylhexyl)oxy]phenyl 4-(decyloxy)-benzoate (also sometimes denoted as 10O7*) [25]. The second and third systems, shown in figures 5 and 6, are homologous series of moderately chiral nFBTFO$_1$M$_7$ and nF$_2$BTFO$_1$M$_7$, both of which are defined by the structure in §1. In addition to the pure compounds with differing tail lengths n, some binary mixtures of homologues have also been studied. In all three systems, the phase diagrams display temperature T as the horizontal axis and composition (roughly related to the magnitude of the coefficient $c_\perp$) as the vertical axis.

Given in table 1 are values of the twist wave vector k_0 in the N* phase, as determined near the N*–I (or N*–BP_I) transition for the three systems described here plus the compound 8BTF$_2$O$_1$M$_7$. The latter compound is part of a homologous series that exhibits TGB_C but not TGB_A phases; indeed for all investigated homologues with $n \geqslant 7$ there is a SmC* phase but no SmA phase [34, 35]. 8BTF$_2$O$_1$M$_7$ is like the structure in §1 with X, Y = H and *two* fluorines on the last ring (chiral methylheptyloxyl end). It must be kept in mind that the width of the N* phase varies, so T_{N^*I} lies closer to the temperature range of TGB and smectic phases in some cases than in others. If the N* range is small, the listed k_0 values 'at' T_{N^*I} are lower bounds; see footnote a in table 1. Also included in table 1 are $2\pi/P$ values at the temperature of the C_p(N*–N_L^*) maximum and in the SmC* phase if it occurs, as well as $(k_0/q_0)^{2/3}$ values. The latter should determine the maximum width of the TGB_A phase via equation (1). Values of the chiral field $h = k_0 K_2$ are not given in the table since good values of the twist elastic constant K_2 are not available. The entries in table 1 show mild trends in k_0 and $(k_0/q_0)^{2/3}$ for the three types of tolan derivatives at any given chain length n. However, the trends in $(k_0/q_0)^{2/3}$ are not strong enough to explain the greater width of the TGB_A phase in nF$_2$BTFO$_1$M$_7$ relative to that in nFBTFO$_1$M$_7$. Experimentally, the values of $\Delta T(\max)$ are ~ 3.8 K for nFBTFO$_1$M$_7$ in figure 5 and ~ 5.4 K for nF$_2$BTFO$_1$M$_7$ in figure 6.

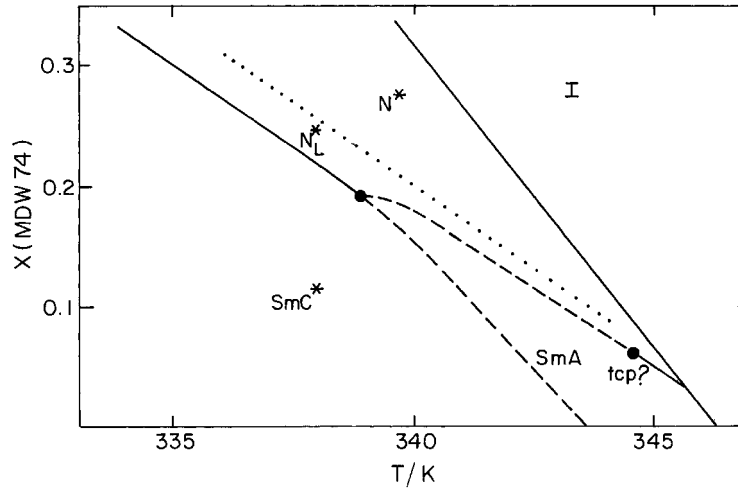

Figure 4. Partial phase diagram for MDW74 + W82 mixtures [25], where X is the weight percent of MDW74. Dashed lines = second order, solid lines = first order, dotted line = proposed nontransitional N*–N_L^* evolution. The tricritical N*–SmA point (denoted as tcp?) near the N*–SmA–I triple point is expected [32] but not confirmed experimentally. The dotted line is based on the location of the maximum in a very broad and rounded C_p feature in the twisted nematic phase.

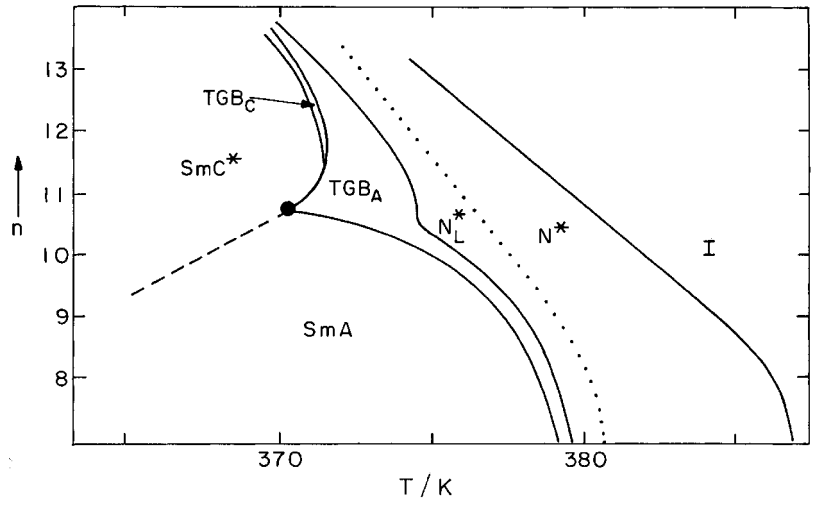

Figure 5. Phase diagram for the chiral series nFBTFO$_1$M$_7$ with slight additive constant shifts of all $n = 9$ and $n = 11$ transition temperatures to eliminate the usual odd–even variation [10]. Dashed line = second order, solid lines = first order, dotted line = nontransitional N*–N$_L^*$ evolution. The character of the TGB$_A$–TGB$_C$ transition is unknown experimentally but presumed to be first order (see text).

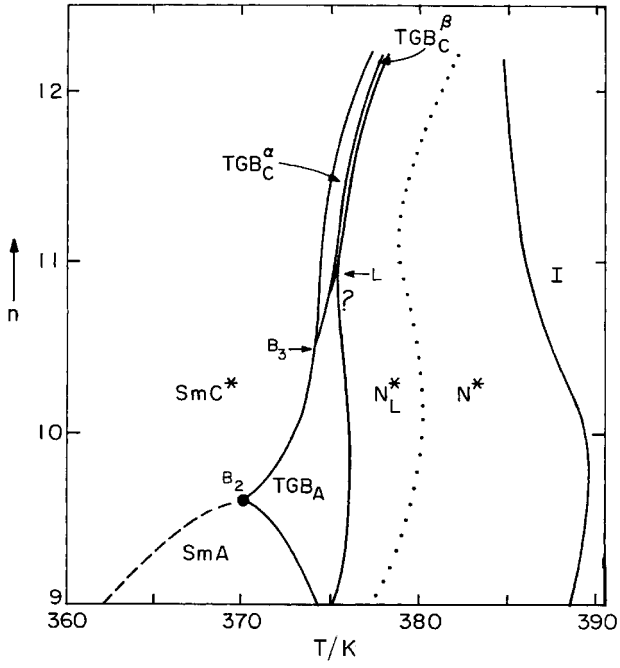

Figure 6. Phase diagram for the chiral series nF$_2$BTFO$_1$M$_7$ [14]. Dashed, solid, and dotted lines have the same meaning as in figures 4 and 5. The topology near the point L is not clear experimentally, and the character of the TGB$_A$–TGB$_C$ transition is unknown for this system. No correction has been applied for the usual odd–even variation in transition temperatures, which is the cause of the wavy nature of the N*–I, N*–N$_L^*$, N$_L^*$–TGB, and SmC*–TGB lines.

A very valuable experiment, not yet carried out, would be a high-resolution study of the phase behaviour in mixtures of R and S enantiomers, ranging from pure R or S to a racemic mixture. This would be especially valuable for a system in which the racemate is close to exhibiting a N–SmA–SmC multicritical point.

In the MDW74 + W82 system (figure 4), there is evidence of a rounded C_p local maximum [25], which can be assigned to N* to N$_L^*$ evolution of short range TGB$_A$ order, but no TGB phases have been identified. A TGB$_A$ phase may exist very close to the N*–SmA–SmC* point since no definitive structural search has been made, but TGB$_C$ is unlikely in view of the fact that the $c_\perp = 0$ locus should lie close to the SmC* boundary as in figures 5 and 6. An equally likely possibility is the absence of TGB$_A$ due perhaps to $\lambda/\xi < 1/\sqrt{2}$ (i.e. type I behaviour) or more probably a very small ΔT(max) from equation (1) so that the TGB$_A$ region is too small to revolve experimentally. It should also be noted that there are no indications of blue phases in this binary mixture [33], which supports the idea that the chirality is fairly low.

Figures 5 and 6 show the temperature–composition (chain length n of tail group) phase diagrams for nFBTFO$_1$M$_7$ and nF$_2$BTFO$_1$M$_7$. The diagram in figure 5 is taken from [10], augmented by recent evidence of a TGB$_C$ phase for $n \geqslant 12$ [15]. The diagram in figure 6 is taken from [14]. High-resolution calorimetric data, established the order of various phase transitions, are available in the case of nFBTFO$_1$M$_7$ for $n = 9$–11 and one binary system with $n = 10.5$ (an equimolar mixture of $n = 10$ and $n = 11$ homologues) [10]. Such high-resolution thermal data are available in the case of nF$_2$BTFO$_1$M$_7$ for $n = 10$–12 [14].

As expected from theory, there is an extensive region of TGB$_A$ phase stability near the underlying fictive N*–SmA–SmC* point. However, there are several apparent differences between figures 5 and 6 and the theoretical figure 3. First, the TGB$_C$ region is dramatically smaller in temperature–composition space than the TGB$_A$ region. One must keep in mind that the TGB$_C$ phase occurs only for $c_\perp < 0$ [12]. Since §2 showed that the

Table 1. Values of $k_0 = 2\pi/P$ in μm^{-1} at T_{N^*I}, and $2\pi/P$ values at $T_{N^*N_L^*}$ and in the SmC* phase (average value). Also listed are $(k_0/q_0)^{2/3}$ values, where q_0 is the SmA wave vector. A dash denotes not applicable; a question mark means data are not available.

Figure	System	$2\pi/P$(SmC*)	$2\pi/P$(N*N$_L^*$)	k_0[a]	$10^2(k_0/q_0)^{2/3}$
4	MDW74 + W82 [33] 20 wt % MDW74	?	25	$\geqslant 25$	?
5	*R*-9FBTFO$_1$M$_7$ [15, 16]	—	18.4	~25–31	6.1–7.0
	10	~5	~23	~24	~6.0
	11	~7	~22	$\geqslant 22$	> 5.8
	12	~6	~21	$\geqslant 24$	~6.3
6	*R*-9F$_2$BTFO$_1$M$_7$ [15, 16]	5.2	~10.5	~26	~6.2
	10	6.9	~22	~29	~6.8
	11	8.2	~18.5	$\geqslant 30$	$\geqslant 7.0$
	12	8.3	~27	$\geqslant 31$	$\geqslant 7.2$
	S-8BTF$_2$O$_1$M$_7$ [34, 35]	~19	~25	28.5	~6.5[b]

[a] The width of the N* + N$_L^*$ regions is less than 6 K in the MDW74 + W82 mixture (3.6 K), 11FBTFO$_1$M$_7$ (5.3 K), and 12FBTFO$_1$M$_7$ (3.9 K). In these three cases, the k_0 values evaluated at T_{N^*I} are lower bounds due to the narrow nematic range. In the two other cases where $\geqslant$ appears, the issue is limited data at high temperatures.

[b] Estimated from $d_A \simeq 0.86l$, where l is the extended configuration molecular length since there is no SmA phase in this compound.

$c_\perp = 0$ locus should lie very close to the SmC* boundary, one would expect a TGB$_C$ topology like that observed. However, there is no evidence in figures 5 and 6, or for any other presently known system, that the TGB$_C$ phase extends down close to the underlying fictive N*–SmA–SmC* multicritical point that would occur in the absence of TGB phases.

Second, note the long narrow 'fingers' of TGB phase that parallel the SmA and SmC* boundaries far from the fictive N–SmA–SmC* point. This is a common feature of many of the TGB phase diagrams studied by the Bordeaux group [8, 9, 15, 16, 35]. Thus the theoretical points B$_I$ and CEP in figure 3 have not been observed experimentally except for the point B$_I$ in the *n*BTFO$_1$M$_7$ series, corresponding to the structure with X, Y = H [15]. In this series, the n = 7–10 homologues exhibit a SmA–N*–(BP)I sequence while n = 11–14 homologues exhibit SmC*–SmA–TGB$_A$–N*–(BP)I. Thus B$_I$ must lie at $n \simeq 10.5$ for *n*BTFO$_1$M$_7$ homologues.

Third, the location of point B$_3$ is not experimentally well determined, but the TGB$_A$–TGB$_C$ boundary seems to approach the TGB$_C$–SmC* boundary tangentially. Figure 6 exhibits a 'point' like the theoretical point L in figure 3 but no detailed high-resolution data are available near L except for 11F$_2$BTFO$_1$M$_7$. Furthermore, no high-resolution experimental data are available for the TGB$_A$–TGB$_C$ transition in either the *n*FBTFO$_1$M$_7$ or *n*F$_2$BTFO$_1$M$_7$ homologous series. Thus the experimental topology near L is unknown. There is, however, a recent high-resolution adiabatic calorimetric study of a fluorinated tolan mesogen that exhibits the SmC*–TGB$_C$–TGB$_A$–BP$_I$ phase sequence [36]. In this case, the TGB$_A$–TGB$_C$ transition is definitely first order with a moderately small latent heat.

Both 11F$_2$BTFO$_1$M$_7$ and 12F$_2$BTFO$_1$M$_7$ exhibit two TGB$_C$ phases, labelled TGB$_C^\alpha$ and TGB$_C^\beta$ in figure 6. No structural information is currently available about TGB$_C^\beta$, but extensive X-ray studies have been made on TGB$_C^\alpha$ in 12F$_2$BTFO$_1$M$_7$ [13, 35]. This Bordeaux X-ray work proves that TGB$_C^\alpha$ is a commensurate TGB$_{Ct}$ phase. Other evidence for two TGB$_C$ phases is provided by 8BTF$_2$O$_1$M$_7$, where these phases are denoted TGB1 and TGB2 [34, 35, 37]. In this case, the available X-ray data show that both TGB$_C$ phases have the same type of layer tilt as in 12F$_2$BTFO$_1$M$_7$: the low temperature TGB1 phase is a commensurate TGB$_{Ct}$ phase and the high temperature TGB2 phase may possibly be an incommensurate TGB$_{Ct}$. It is plausible to associate TGB2 with TGB$_C^\beta$, but this correspondence is not yet established. It should be noted in passing that there is as yet no theoretical explanation for the existence of commensurate TGB structures.

It should be stressed that the *n*BTF$_2$O$_1$M$_7$ series for $n \geqslant 7$ does not exhibit either SmA or TGB$_A$ phases and thus lies fairly far above the fictive N*–SmA–SmC* point. However, there is no narrowing of the total TGB$_C$ range as n increases from 7 to 11 [35] and thus no approach to the theoretical CEP point shown in figure 3. Indeed, it is reported that 16FBTFO$_1$M$_7$ exhibits the sequence SmC*–TGB$_A$–N*–I and 18FBTFO$_1$M$_7$ exhibits the sequence SmC*–TGB$_A$–I [15]. If this is verified by high-resolution structural work, then the TGB$_C$ phase(s) in *n*FBTFO$_1$M$_7$ homologues may lie as a narrow closed region parallel to *part* of the SmC*–TGB$_A$ boundary. It

seems possible that for very large n values nBTFO$_1$M$_7$, nFBTFO$_1$M$_7$ and nF$_2$BTFO$_1$M$_7$ may exhibit a SmC*–I phase sequence with neither N* nor TGB phases [15]. New and careful studies of large n homologues are obviously needed for all three series to confirm or reject this idea.

One interesting issue is the speculation that there may *always* be two TGB$_C$ phases with the higher temperature TGB$_C^{\beta}$ (or TGB2) phase stable over a rather narrow T range. In nF$_2$BTFO$_1$M$_7$, TGB$_C^{\beta}$ exists over only 0.05–0.10 K [14] and was missed in early work. In 8BTF$_2$O$_1$M$_7$, TGB2 is stable over 0.4 K and the entire TGB$_C$ region is wider (1.7 K compared with 0.75–0.82 K in nF$_2$BTFO$_1$M$_7$). Better high-resolution scattering studies are needed to characterize the TGB$_C^{\beta}$ and TGB2 structures and establish whether they are the same, and if either or both correspond to TGB$_{2q}$ [30] or perhaps to a TGB$_C$ structure with 'curved' smectic layers [38].

A final difference between experiment and the mean-field theory shown in figure 3 is the character of the phase transitions. Both theory and experiment agree that the SmA–SmC* transition is second order and the SmC*–TGB$_A$, SmC*–TGB$_C$, SmC*–N* transitions are all first order. The mean-field theoretical prediction that SmA–TGB$_A$, TGB$_A$–N* and TGB$_C$–N* transitions are second order disagrees with experiments where high-resolution data exist. The latter data show, as indicated in figures 5 and 6, that these three transitions are strongly first order with moderate or small latent heats [10, 14]. Table 2 summarizes the comparison of current theory and experiment with respect to the order of phase transitions and lists typical transition enthalpies. It should be mentioned that Renn [12] does allow the theoretical possibility of a first order SmA–TGB$_A$ transition if the SmA layer compressibility is sufficiently large. The experimental character of the N*–SmA transition in nBTFO$_1$M$_7$ is not yet established, but N–SmA transitions in nonchiral systems with nematic ranges wider than about 2–3 K are known to be second order [32]. As noted in figure 4, there might be a tricritical point and crossover to first order N*–SmA due to de Gennes smectic–nematic coupling when the N* range becomes quite small [32], but this has no connection to point B$_1$. The predicted first order N*–SmA line below B$_1$ in figure 3 is based on a theoretical analogy to the type-I superconducting transition (in contrast to type-II behaviour above B$_1$, where a TGB phase is expected) [39]. This N*–SmA transition is not expected to be as strongly first order as the normal-superconductor type-I transition since fluctuations can significantly unwind the helix. Indeed, theoretical estimates of the N*–SmA latent heat yield extremely small values [39]. The last transition to consider is TGB$_A$–TGB$_C$, where theory predicts second order Ising behaviour or perhaps a weak first order transition when fluctuations are taken into account [11, 12]. Unfortunately, despite efforts to study a 10.75F$_2$BTFO$_1$M$_7$ mixture [14], no experimental evidence is available from the nF$_2$BTFO$_1$M$_7$ series about the nature of the TGB$_A$–TGB$_C$ transition. However, the data in [36] establish that the TGB$_A$–TGB$_C$ transition is first order in the one case that has been well characterized. It should be noted in passing that the non-transitional character of the N*–N$_L^*$ short range evolution (dotted lines in figures 4–6) is predicted theoretically [17] and confirmed experimentally [10, 14, 25].

Table 2. Comparison of transition order predicted by MF theory [11, 12, 17] with that observed experimentally [10, 14, 36]. The enthalpies cited are latent heats ΔH in the case of the first order (1st) transitions and the integrated area δH for the non-transitional N*–N$_L^*$ feature.

	Order of transition		
Transition	Theory	Exp.	Typical enthalpy/mJ g^{-1}
N$_L^*$–N*	non	non	300–1800
TGB$_A$–N$_L^*$	2nd[a]	1st	~0–8
TGB$_C$–N$_L^*$	2nd[a]	1st[c]	140–300
TGB$_C$–TGB$_A$	2nd[a]	1st	~90
SmA–TGB$_A$	2nd[b]	1st	~40
SmC*–TGB$_A$	1st	1st	~70
SmC*–TGB$_C$	1st	1st	40–125

[a] It is theoretically possible that these transitions may become weakly first order if fluctuations are taken into account.
[b] A first order transition is predicted if the SmA layer compressibility is large enough [12].
[c] Two closely spaced first order transitions (TGB$_C^{\alpha}$–TGB$_C^{\beta}$–N$_L^*$) are observed experimentally; see text and figure 6.

5. Summary

The basic theoretical TGB phase diagram shown in figure 3, based on the theory in [11, 12, 29, 30] and augmented by the N*–N$_L^*$ feature predicted in [17], is topologically quite close to typical experimental diagrams. The differences, rather than the similarities, are stressed below as a stimulus for new experimental and theoretical work.

As a starting point the *nonchiral* Chen–Lubensky model fails to represent two significant experimental features of nonchiral N–SmA–SmC diagrams: (i) the N–SmA–SmC point is simultaneously a Lifshitz point and a Landau tricritical point and (ii) the $c_{\perp} = 0$ locus lies very close the N–SmC boundary.

The Renn–Lubensky mean-field *chiral* version of the Chen–Lubensky model differs from experiment in five ways:

(1) The extents of the TGB_C and TGB_A stability fields appear theoretically very similar whereas the experimental $T-X$ area is much smaller for TGB_C than TGB_A. Also the TGB_C phase appears experimentally at compositions far from that of the fictive N*–SmA–SmC* point, and TGB_A dominates the fictive N*–SmA–SmC* region. Both of these effects may be due to having the $c_\perp = 0$ locus lie very close to the SmC* boundary.

(2) TGB_A and TGB_C phases extend experimentally far below and above the fictive N*–SmA–SmC* region with long 'fingers' following the SmA and SmC* boundaries. As a result, the point CEP in figure 3 has never been seen experimentally and the point B_I occurs only in rare cases.

(3) The experimental topology at the junction of TGB_A–TGB_C and TGB_C–SmC* transition lines (tangency) is not reflected in the theory.

(4) There appear to be two experimental TGB_C phases—TGB_C^α (TGB1) at lower temperatures near SmC* and TGB_C^β (TGB2) at higher temperatures near N_L^*. The structural difference between these two phases is not yet known, but TGB_C^α (TGB1) is a commensurate TGB_{Ct} phase. A theoretical explanation for the existence of commensurate TGB structures is still needed.

(5) The predicted second order character of the SmA–TGB_A, TGB_A–TGB_C, TGB_A–N_L^* and TGB_C–N_L^* transitions is contradicted by experimental proof of first order transitions in all four cases. However, analogies with superconductors suggest that fluctuations can drive both the TGB_A–N_L^* and TGB_C–N_L^* transitions first order. Thus the 'mean-field' theoretical results in [11, 12] may need to be modified. In this context, it should be pointed out that the experimental latent heats given in table 2 are very small for TGB_A–N_L^*, small for SmA–TGB_A, SmC*–TGB_A, SmC*–TGB_C^α, TGB_C–TGB_A, and moderate for the sum of TGB_C^α–TGB_C^β–N_L^* (140–300 mJ g^{-1}, with TGB_C^α–TGB_C^β only ~15% of the total). These latent heats can be compared to the substantial non-transitional excess enthalpy δH associated with the N*–N_L^* evolution of short range TGB order: $\delta H = \int \Delta C_p(\mathrm{N^*}\text{–}N_L^*)\,dT$. Such δH values range from 1400 mJ g^{-1} in $10F_2BTFO_1M_7$ to 280 mJ g^{-1} in $12F_2BTFO_1M_7$ and from 1800 mJ g^{-1} in $9FBTFO_1M_7$ to 820 mJ g^{-1} in $11FBTFO_1M_7$ [10, 14]. Thus there is considerable local TGB order in the N_L^* region and only small enthalpy changes occur on going from N_L^* via TGB_A or TGB_C to SmA or SmC*. Naturally scattering experiments are sensitive to these ordering transitions since long range order is appearing or changing. However, a more detailed theory is needed for TGB phase transitions in which local (short range) smectic order of the N_L^* type is included.

Finally, it seems worth mentioning that the temperature dependence of the helical pitch $|dP/dT|$, and thus the variation in $2\pi/P$ as a function of T, differs in the TGB_A and TGB_C phases [15, 16, 34]. $|dP/dT|$ grows continuously larger on cooling from N* to N_L^* to TGB_A, but there is a sudden change when the TGB_C phase is entered. Either there is a sharp kink in P versus T with $|dP/dT|$ having a much larger and roughly constant value in the TGB_C phase, or there is a jump in P at the transition into the TGB_C phase followed again by a large constant $|dP/dT|$ value in the TGB_C phase. Naturally, $P = 0$ in the SmA phase and P is roughly constant in the SmC* phase.

The author wishes to thank P. Barois, T. C. Lubensky, L. Navailles, H. T. Nguyen, and R. Pindak for helpful and stimulating discussions and M. D. Wand for making pitch measurements in a MDW74 + W82 mixture. This work was supported by the MRSEC program of the National Science Foundation under grant DMR-9400334.

References

[1] Renn, S. R., and Lubensky, T. C., 1988, *Phys. Rev. A*, **38,** 2132.
[2] Lubensky, T. C., and Renn, S. R., 1990, *Phys. Rev. A*, **41,** 4392.
[3] Goodby, J. W., Waugh, M. A., Stein, S. M., Chin, E., Pindak, R., and Patel, J., 1989, *Nature*, **337,** 449.
[4] Huang, C. C., Lin, D. S., Goodby, J. W., Waugh, M. A., Stein, S. M., and Chin, E., 1989, *Phys. Rev. A*, **40,** 4153.
[5] Strajer, G., Pindak, R., Waugh, M. A., and Goodby, J. W., 1990, *Phys. Rev. Lett.*, **64,** 1545.
[6] Ihn, K. J., Zasadzinski, A. N., Pindak, R., Slaney, A. J., and Goodby, J., 1992, *Science*, **258,** 275.
[7] Goodby, J. W., Nishiyama, I., Slaney, A. J., Booth, C. J., and Toyne, K. J., 1993, *Liq. Cryst.*, **14,** 37.
[8] Bouchta, A., Nguyen, H. T., Achard, M. F., Hardouin, F., Destrade, C., Twieg, R. J., Maaroufi, A., and Isaert, N., 1992, *Liq. Cryst.*, **12,** 575.
[9] Nguyen, H. T., Bouchta, A., Navailles, L., Barois, P., Isaert, N., Twieg, R. J., Maaroufi, A., and Destrade, C., 1992, *J. Phys. II Fr.*, **2,** 1889.
[10] Chan, T., Garland, C. W., and Nguyen, H. T., 1995, *Phys. Rev. E*, **52,** 5000.
[11] Renn, S. R., and Lubensky, T. C., 1991, *Mol. Cryst. liq. Cryst.*, **209,** 349.
[12] Renn, S. R., 1992, *Phys. Rev. A*, **45,** 953.
[13] (*a*) Navailles, L., Barois, P., and Nguyen, H. T., 1993, *Phys. Rev. Lett.*, **71,** 545; (*b*) Navailles, L., Pindak, R., Barois, P., and Nguyen, H. T., 1995, *Phys. Rev. Lett.*, **74,** 5224.
[14] Navailles, L., Garland, C. W., and Nguyen, H. T., 1996, *J. Phys. II Fr.*, **6,** 1243.

[15] Bouchta, A., Nguyen, H. T., Navailles, L., Barois, P., Destrade, C., Bougrioua, F., and Isaert, N., 1995, *J. mater. Chem.*, **5,** 2079.
[16] Bougrioua, F., 1997, PhD thesis, University of Lille, France (unpublished).
[17] Kamien, R. D., and Lubensky, T. C., 1993, *J. Phys. I Fr.*, **3,** 2131.
[18] (*a*) Martinez-Miranda, L. J., Kortan, A. R., and Birgeneau, R. J., 1986, *Phys. Rev. Lett.*, **56,** 2264; (*b*) Martinez-Miranda, L. J., Kortan, A. R., and Birgeneau, R. J., 1987, *Phys. Rev. A*, **36,** 2372.
[19] (*a*) Garland, C. W., and Huster, M. E., 1987, *Phys. Rev. A*, **35,** 2365; (*b*) Huster, M. E., Stine, K. J., and Garland, C. W., 1987, *Phys. Rev. A*, **36,** 2364.
[20] (*a*) De Hoff, R., Biggers, R., Brisbin, D., and Johnson, D. L., 1982, *Phys. Rev. A*, **25,** 472; (*b*) Safinya, C. R., Martinez-Miranda, L. J., Kaplan, M., Litster, J. D., and Birgeneau, R. J., 1983, *Phys. Rev. Lett.*, **50,** 56.
[21] Thoen, J., and Parret, R., 1989, *Liq. Cryst.*, **5,** 479.
[22] Brisbin, D., Johnson, D. L., Fellner, H., and Neubert, M. E., 1983, *Phys. Rev. Lett.*, **50,** 178.
[23] Shashidhar, R., Ratna, B. R., and Krishna Prasad, S., 1984, *Phys. Rev. Lett.*, **53,** 2141.
[24] Chen, J.-C., and Lubensky, T. C., 1976, *Phys. Rev. A*, **14,** 1202.
[25] Wen, X., Garland, C. W., and Wand, M. D., 1990, *Phys. Rev. A*, **42,** 6087 and references therein.
[26] Swift, J., 1976, *Phys. Rev. A*, **14,** 2274.
[27] Hill, J. P., Keimer, B., Evans-Lutterodt, K. W., Birgeneau, R. J., and Garland, C. W., 1989, *Phys. Rev. A*, **40,** 4625.
[28] Navailles, L., Pansu, B., Gorre-Talini, L., and Nguyen, H. T., 1998, *Phys. Rev. Lett.*, **81,** 4168.
[29] Dozov, I., 1995, *Phys. Rev. Lett.*, **74,** 4245. In this paper, the TGB_{Ci} phase is called a twist-melted-grain-boundary (TMGB) phase.
[30] Luk'yanchuk, I., 1998, *Phys. Rev. E*, **57,** 574.
[31] Lubensky, T. C., private communication. The basic premise for this result is based on the theory of SmC elasticity and dislocations given in Hatwalne, Y., and Lubensky, T. C., 1995, *Phys. Rev. E*, **52,** 6240.
[32] (*a*) Thoen, J., 1992, *Calorimetric Studies of Liquid Crystal Phase Transitions: Steady State Adiabatic Techniques*, in *Phase Transitions in Liquid Crystals*, edited by S. Martellucci, *NATO ASI Proceedings of an International School held in Erici* (New York: Plenum); (*b*) Garland, C. W., and Nounesis, G., 1994, *Phys. Rev. E*, **49,** 2964. The only known example of a first order N–SmA transition occuring in systems with nematic ranges > 3 K is in 4O.8 + 6O.8 mixtures, where the N–SmA tricritical point occurs for a 7.75 K nematic range; see details given in (*a*).
[33] Wand, M. D., private communication.
[34] Navailles, L., Nguyen, H. T., Barois, P., Isaert, N., and De Lord, P., 1996, *Liq. Cryst.*, **20,** 653.
[35] Navailles, L., 1994, PhD thesis, University of Bordeaux I, France (unpublished).
[36] Young, M., Pitsi, G., Li, M.-H., Nguyen, H.-T., Jamee, P., Sigaud, G., and Thoen, J., 1998, *Liq. Cryst.*, **25,** 387.
[37] Iannacchione, G. S., and Garland, C. W., 1998, *Liq. Cryst.* (in the press).
[38] Dozov, I., private communication.
[39] Lubensky, T. C., 1975, *J. Phys. (Paris)*, **36,** C1.